RAPID COMMUNICATIONS

PHYSICAL REVIEW E VOLUME 51, NUMBER 4 APRIL 1995

Numerical study of cylindrically confined nematic liquid crystals

Renata-Maria Marroum, Germano S. Iannacchione, Daniele Finotello, and Michael A. Lee
Department of Physics and Liquid Crystal Institute, Kent State University, Kent, Ohio 44242
(Received 1 September 1994)

Using a Landau–de Gennes free energy, we present a systematic numerical study of nematic liquid crystals confined in a cylindrical cavity. We discuss the nematic to isotropic phase transition of 4-*n*-pentyl-4′-cyanobiphenyl (5CB) in a cylinder with a large length to width ratio and consider the effects of different surface anchoring interactions and director configurations. We calculate the temperature profile of the scalar orientational order parameter, heat capacity and latent heat, finding excellent agreement with recent experimental studies, and suggest the practical applicability of the model.

PACS number(s): 61.30.Gd, 64.70.Md, 74.20.De

There is a need to increase the quantitative understanding of finite size, confinement, and surface effects, as they play a significant role in many liquid crystal device applications such as display cells and light shutter devices [1]. Such systems are interesting because the bulk nematic to isotropic (*N-I*) transition is weakly first order, and thus sensitive to external fields and boundary effects. Studies of nematic liquid crystals in cylindrical cavities permit the modeling of noncylindrical confining geometries as a collection of cylindrical pores [2], allowing for a better theoretical understanding. This numerical study is an attempt using a full Landau–de Gennes (LdG) free energy that includes bulk terms, spatial variations of the order parameter and director, as well as surface ordering and disordering interactions. This work is aimed at exploring *both* the orientational and thermodynamic properties of nematic liquid crystals confined to cylindrical pores.

Recent experimental work [3–6] revealed interesting phenomena that have been accounted for via simple theoretical approaches [7–10]. Heat capacity measurements [3] on nematic liquid crystals (LCs) confined to 0.1 μm radii cylindrical pores of aluminum oxide Anopore membranes found the *N-I* transition to be no longer divergent but rounded, broadened, and shifted to lower temperature. These effects were dependent on the director configuration in the pores that was varied by surface treatment. Similar shifts in the transition temperature T_C were observed by optical microscopy [4] on similar pore size polycarbonate Nuclepore membranes. Deuterium NMR studies probing the orientational order and direct configurations carried out on both Anopore [5] and Nuclepore [6] found several types of director configurations, configurational transitions, and surface induced nematic ordering in the isotropic phase, dependent on surface treatment.

A comprehensive theoretical treatment has been available through a full LdG approach [7] but it is often simplified [8,9]. With the availability of powerful computational resources, the ability to numerically implement a complete LdG approach allows the various experimental observations to be modeled under a unified theory. Here, we attempt to bridge the gap between the various experimental and theoretical results. The resulting numerical method might be applicable for other geometries and LCs, hopefully becoming a useful tool in the understanding of confined LCs.

We focus on uniaxial LCs confined to cylindrical cavities of 0.1 μm radii which allows a direct comparison with recent experimental work. Previous studies of the *N-I* transition as a function of pore size and anchoring strength [11] found that below some critical radii, $R<R_C$, it becomes continuous as found for planar confinement below some critical thickness [8,9]. Here, we describe the model used, then discuss the results in comparison with experiments for $R=0.1$ μm, which is well below R_C for the given substrate surface interactions.

The extended LdG model, described elsewhere [7,11], is based on the expansion of the free energy in a power series of the tensor order parameter, $\mathbf{Q}(\mathbf{r})$, which characterizes the alignment of the LC molecules. For the uniaxial case, it is a real and traceless symmetric tensor: $\mathbf{Q}(S(\mathbf{r}),\mathbf{n}(\mathbf{r}))=\frac{1}{2}S(3n_in_j-\delta_{ij})$, where S is the scalar order parameter and $\mathbf{n}$ is a unit vector describing the director field. In the nematic phase, the director field within a cylindrical cavity is given by

$$\mathbf{n}=\mathbf{i}\sin\Omega\cos\Phi+\mathbf{j}\sin\Omega\sin\Phi+\mathbf{k}\cos\Omega, \tag{1}$$

where Ω is the angle between $\mathbf{n}$ and the axis of the cylinder, $\mathbf{k}$, and Φ is the angle between $\mathbf{n}$ and $\mathbf{i}$, a unit vector in the plane perpendicular to $\mathbf{k}$. Both the scalar order parameter and the director are allowed to be spatially dependent.

The total Helmholtz free energy of a uniaxial nematic LC in the absence of external electric and magnetic fields is given by

$$F=\int_V d^3\mathbf{r}[f_o+f_h+f_e-GS+\tfrac{1}{2}US^2 +(\tfrac{3}{2}GS-\tfrac{3}{8}US^2)(\sin^2\theta)\delta(r-R)], \tag{2}$$

where f_o, f_h, and f_e are the regular background (order parameter independent), the bulk (homogeneous), and the spatial (elastic) parts of the free energy density, respectively. The terms containing G and U [1,2,8,10] are the ordering and disordering surface terms, respectively, with $\theta=\pi/2-\Omega$ at the surface. The US^2 term describes the disordering effects of surface induced deformations; the $-GS$ term represents the ordering effect of the surface interactions. Explicitly, the bulk contribution is

$$f_h=\tfrac{3}{4}A_o(T-T^*)S^2+\tfrac{1}{4}BS^3+\tfrac{9}{16}CS^4, \quad (3)$$

where A_o, B, and C are phenomenological material parameters and T^* is the lowest stable temperature of the isotropic phase (supercooling temperature).

The elastic contribution consists of $f_e=f_{\text{splay}}+f_{\text{twist}}+f_{\text{bend}}+f_{\text{saddle-splay}}+f_{\text{spatial}}$, where the different terms, written in terms of the Frank elastic energy parameters [7,12], correspond to

$$f_{\text{splay}}=\frac{9}{4}\left(L_1+\frac{L_2+L_3}{2}\right)S^2(\nabla\cdot\hat{\mathbf{n}})^2=\tfrac{1}{2}K_{11}(\nabla\cdot\hat{\mathbf{n}})^2, \quad (4a)$$

$$f_{\text{twist}}=\tfrac{9}{4}L_1S^2(\hat{\mathbf{n}}\cdot\nabla\times\hat{\mathbf{n}})^2=\tfrac{1}{2}K_{22}(\hat{\mathbf{n}}\cdot\nabla\times\hat{\mathbf{n}})^2, \quad (4b)$$

$$f_{\text{bend}}=\frac{9}{4}\left(L_1+\frac{L_2+L_3}{2}\right)S^2(\hat{\mathbf{n}}\times\nabla\times\hat{\mathbf{n}})^2=\tfrac{1}{2}K_{33}(\hat{\mathbf{n}}\times\nabla\times\hat{\mathbf{n}})^2, \quad (4c)$$

$$f_{\text{saddle-splay}}=-\frac{9}{4}\left(L_1+\frac{L_3}{2}\right)S^2\nabla[\hat{\mathbf{n}}(\nabla\cdot\hat{\mathbf{n}})+\hat{\mathbf{n}}\times(\nabla\times\hat{\mathbf{n}})]$$
$$=\tfrac{1}{2}K_{24}\nabla[\hat{\mathbf{n}}(\nabla\cdot\hat{\mathbf{n}})+\hat{\mathbf{n}}\times(\nabla\times\hat{\mathbf{n}})]. \quad (4d)$$

The spatial term, having contributions from ∇S and its coupling to $\mathbf{n}$, describes the spatial variations of the scalar order parameter and the director and is given by

$$f_{\text{spatial}}=\frac{3}{4}\left(L_1+\frac{L_2+L_3}{2}\right)(\nabla S)^2+\tfrac{3}{8}(L_1+L_3)(\hat{\mathbf{n}}\cdot\nabla S)$$
$$+\frac{3}{2}\left(L_2-\frac{L_3}{2}\right)S(\nabla S\cdot\hat{\mathbf{n}})$$
$$+\frac{3}{2}\left(\frac{L_2}{2}-L_3\right)S(\hat{\mathbf{n}}\times\nabla\times\hat{\mathbf{n}})\cdot\nabla S, \quad (4e)$$

where L_1, L_2, and L_3 are phenomenological material parameters. Taking $L_1\neq 0$ and $L_2=L_3=0$, it reduces to the single elastic constant approximation where $K_{11}=K_{22}=K_{33}$, often used for planar geometries [8,9]. For the surface interaction terms, previous work in planar systems used $G\neq U\neq 0$ [9], while $G\neq 0$ and $U=0$ for curved geometries [12]. Here, both G and U vary.

The numerical implementation directly minimizes the total free energy as a function of temperature. This is done using finite differences and then minimizing the resulting discretized free energy for the equilibrium order parameter tensor by the damped Newton method [11,13]. From the minimized total free energy, the resulting equilibrium order parameter is known and several experimental response functions are calculated and compared directly with recent work [3,5,6]. From $\mathbf{Q}$, the ^{2}H-NMR quadrupole splitting may be calculated by $\Delta\nu=\frac{1}{2}\Delta\nu_0 S(3\cos^2\theta_B-1)$ where θ_B is the angle between $\mathbf{n}$ and the static magnetic field [14]. The heat capacity is calculated, $C=-T(\partial^2F/\partial T^2)$, as well as the latent heat, $l_{N\text{-}I}=T_c(\Delta S)$, where $S=\partial F/\partial T$ is the entropy and ΔS is the change in entropy at the N-I transition [15].

We study 4-n-pentyl-4′-cyanobiphenyl (5CB) confined to 0.1 μm radii cylindrical pores having two different director orientations at the pore wall, parallel or tangential (axial) and perpendicular or homoetropic (radial). For 5CB, we use $A_0=8.67\times10^5$ J/K m^3, $B=2.12\times10^6$ J/m^3, $C=1.74\times10^6$ J/m^3, and $T^*=307.14$ K, which is $\sim$1.1 K below $T^b_{N\text{-}I}$, the bulk N-I transition temperature [16]. For the elastic constants, we use the approximation $L_2+L_3=2.5L_1$, which is in reasonable agreement with the experimental range [17]. Using $L_1=0.26\times10^{-11}$ J/m and letting $L_2=L_3$, this corresponds to $K_{11}=K_{33}$ and $K_{24}/K=1.4$. For the radial case (experimentally obtained after lecithin treatment of the pores), we use strong surface anchoring parameters with $G=8.5\times10^{-3}$ J/m^2 and $U=7.0\times10^{-3}$ J/m^2 [1,9,10]. For the axial case (untreated Anopore), a weaker surface ordering of $G=6.0\times10^{-4}$ J/m^2 is used, an order of magnitude smaller than in the radial case, consistent with NMR results [5]. To compare with bulk, G and U are set to zero, thus eliminating the surface terms from the free energy. The ratio G/U describes the competition between surface ordering and disordering effects.

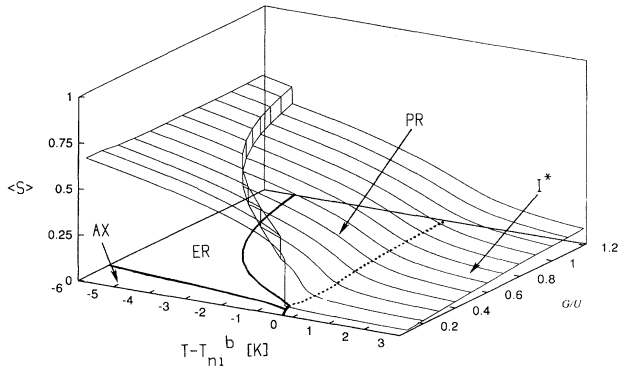

FIG. 1. Three-dimensional plot of the average order parameter, $\langle S\rangle$, vs $T-T^b_{N\text{-}I}$ vs G/U.

Several configurations are possible in cylindrical cavities [5,6,12,18]. It has been shown that for $R<R_C$, there is a discontinuous transition from the escaped radial (ER) configuration to an isotropic phase with an ordered surface region, I^* [11]. These are shown in the inset to Fig. 2. As the cavity radius decreases, equivalent to G/U increasing, there are three transition sequences in the phase diagram; see $T-T^b_{N\text{-}I}$ G/U plane in Fig. 1. The first is a continuous transition from an axial or AX (inset to Fig. 2) case to I^* for $G/U\leq 0.1$. For $0.1\leq G/U\leq 0.13$, there is a phase transition sequence of AX to ER to I^*, all discontinuously. For $G/U>0.13$ a discontinuous transition from ER to planar radial (PR) (inset to Fig. 2), where a line defect is formed at the center, occurs below a continuous PR to I^* transition. The last transition involves a gradual increase in the core size beginning with the line defect in the PR phase.

The test cases, $G/U=1.214$ for the radial and $G/U=0.08$ for the axial, are shown in Fig. 2. There is a discontinuous configurational transition 7 K below $T^b_{N\text{-}I}$. Such an ER configuration was observed 10.5 K below $T^b_{N\text{-}I}$ for 5CB in 0.1 μm Nuclepore [19]. In both the axial and radial cases, we find a boundary layer remaining deep in the

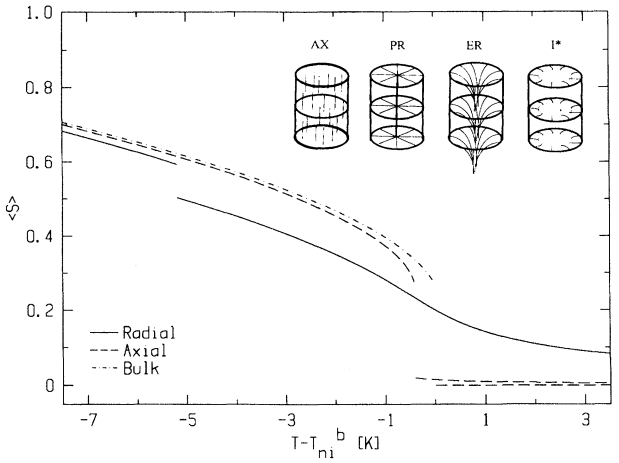

FIG. 2. Plot of $\langle S\rangle$ vs $T\text{-}T^{b}_{N\text{-}I}$ for bulk, axial, and radial cylindrical cases. The axial and radial cases correspond to $G/U=0.08$ and 1.214, respectively. Also shown are the possible distinct director configurations in a cylindrical geometry.

isotropic phase, with the radial value being an order of magnitude larger (0.1) than the axial (0.01) at the same T. The ER to PR transition involves small changes in energy, and thus would be very difficult to observe thermodynamically.

The computed heat capacity [20] as a function of reduced temperature t, $t=(T-T_C)/T_C$, for the three cases is shown in Fig. 3 (top). Comparing with bulk, the axial case retains its first order nature, but occurs at a slightly lower temperature, $T_C=307.84$ K. In stark contrast, the radial case shows a significant peak suppression, broadening, and appears to be continuous; it occurs at an even lower temperature, $T_C=307.34$ K. This is in good agreement with the experimental data [3] shown in Fig. 3 (bottom), confirming a narrow pore size distribution for Anopore.

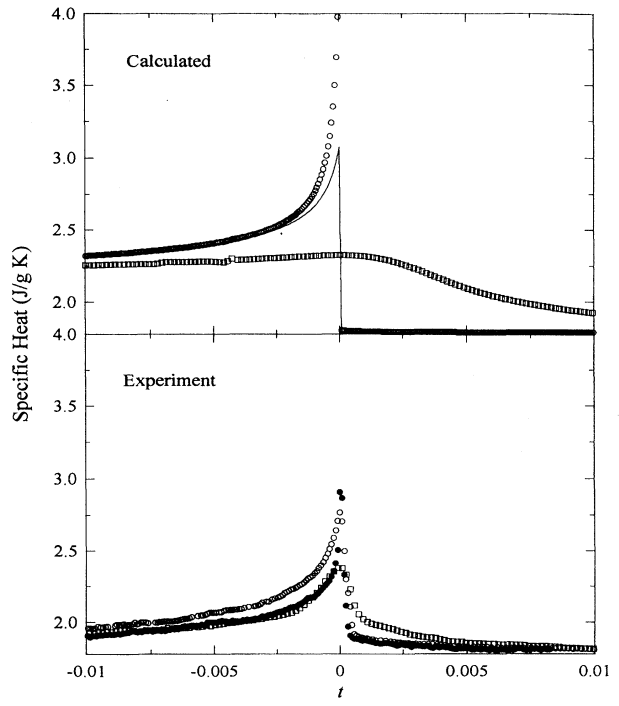

FIG. 3. Calculated (top) and experimental (bottom) heat capacities for bulk 5CB (solid line and ●), axially (○), and radially (□) confined in Anopore.

At the same t, on the nematic side, the heat capacity decreases from the axial to bulk then to radial; on the isotropic side, the heat capacity is higher for the radial than the axial, both above bulk. Again, this is in good agreement with experiment. For $t<0$, the smaller heat capacity of the radial alignment results from the stronger pinning of the molecules to the wall; thus, a smaller fraction of the molecules participates in the ordering as compared with the axial case, where a larger portion of the molecules are free to participate. For $T>T_C$ ($t>0$), there is a significant amount of specific heat present in the system. Our results show that the minimum free energy for the radial configuration is that of a PR, where the nematic material is all aligned perpendicular to the boundary. However, within the temperature range shown in Fig. 3 (top), the molecules do not escape along **k** (ER); instead, a line defect at the center is formed. The broad transition peak is due to a gradual growth in the size of this line defect into a finite isotropic core. This explains the large difference in the heat capacity between the radial and the bulk for $t>0$. The theory does not take into account the two-phase coexistence region at a first order phase transition which would round the divergent nature of the bulk and axial cases while retaining a certain sharpness in the radial case [21].

Finally, latent heat (l_t) values are calculated for bulk and confined cases. For bulk 5CB and 4-heptyl-4′-cyanobiphenyl (7CB), l_t is 1.467 and 2.197 J/g, respectively; both are within 6% of the experimental values of 1.56 and 2.08 J/g, respectively [22]. For the axially confined 5CB, the calculated latent heat decreases to 1.123 J/g as expected since the residual $\langle S\rangle$ in the isotropic phase decreases the jump $\langle S\rangle$ at T_C further weakening this weakly first order transition. For the radially confined 5C, the latent heat nearly disappears at T_C being only 0.01 J/g as a consequence of the continuous nature of the transition. The results for the latent heat of the confined cases need to be experimentally verified.

In summary, we performed a numerical minimization of the full LdG free energy in which both the scalar and orientational order parameters were allowed to vary spatially. We showed that the N-I transition in 0.1 μm radii cavities is strongly affected by the surface conditions of the walls, and the results are in excellent quantitative agreement with experiment. The numerical study should be extended to allow the order parameter to vary with the polar angle. This would permit us to incorporate the planar polar (PP) case, where the two line defects (with strength $\frac{1}{2}$) are present and are located at the boundary. For small radii the PP configuration is essentially more favorable over the PR. This has yet to be investigated. It would also be useful to perform ^{2}H-NMR studies with a higher temperature resolution to get a more quantitative analysis of the configurational transitions. NMR results combined with an analysis of the full free energy and an additional theoretical analysis of self-diffusion would

provide an unambiguous assignment of director configuration information. It would also be useful to carry out specific heat measurements with lecithin treated larger cavity sizes to investigate the change in the configurational transitions.

We thank E. C. Gartland and C. Greeff for many useful discussions, and the generous collaboration of computational resources from the Ohio Supercomputer Center. This work was supported by NSF-ALCOM Grant No. DMR-8920147.

[1] B. Jerome, Rep. Prog. Phys. **54**, 391 (1991).

[2] G. S. Iannacchione, G. P. Crawford, S. Zumer, J. W. Doane, and D. Finotello, Phys. Rev. Lett. **71**, 2595 (1993).

[3] G. S. Iannocchione and D. Finotello, Liq. Cryst. **14**, 1135 (1993); Phys. Rev. Lett. **69**, 2094 (1992).

[4] M. Kuzma and M. M. Labes, Mol. Cryst. Liq. Cryst. **100**, 103 (1983).

[5] G. P. Crawford, R. J. Ondris-Crawford, S. Zumer, and J. W. Doane, Phys. Rev. Lett. **70**, 1838 (1993); G. P. Crawford, R. Stannarius, and J. W. Doane, Phys. Rev. A **44**, 2558 (1991).

[6] R. J. Ondris-Crawford, G. P. Crawford, S. Zumer, and J. W. Doane, Phys. Rev. Lett. **70**, 194 (1993); G. P. Crawford, D. K. Yang, S. Zumer, D. Finotello, and J. W. Doane, *ibid.* **66**, 723 (1991).

[7] P. de Gennes and J. Post, *The Physics of Liquid Crystals*, 2nd ed. (Oxford University Press, New York, 1993); Phys. Rev. A **43**, 2943 (1991).

[8] P. Sheng, Phys. Rev. Lett. **37**, 1059 (1976); Phys. Rev. A **26**, 1610 (1982).

[9] H. Yokoyama, J. Chem. Soc. Faraday Trans. 2 **84**, 1023 (1988).

[10] A. Poniewierski and T. J. Sluckin, Mol. Cryst. Liq. Cryst. **179**, 349 (1990); Liq. Cryst. **2**, 281 (1987); T. J. Sluckin and A. Poniewierski, in *Fluid Interfacial Phenomena*, edited by C. A. Croxton (Wiley, New York, 1983), Chap. 5.

[11] R-M. Marroum, E. C. Gartland, and Michael A. Lee (unpublished).

[12] S. Krajl and S. Zumer, Liq. Cryst. **15**, 521 (1993); S. Krajl, S. Zumer, and D. W. Allender, Phys. Rev. A **43**, 2943 (1991).

[13] E. C. Gartland, Jr., P. Palffy-Muhoray, and R. S. Varga, Mol. Cryst. Liq. Cryst. **199**, 429 (1991).

[14] A. Golemme, S. Zumer, J. W. Doane, and M. E. Neubert, Phys. Rev. A **37**, 559 (1988); J. W. Doane, in *Magnetic Resonance of Phase Transitions*, edited by F. J. Owens, C. P. Poole, Jr., and H. A. Farah (Academic, New York, 1974), Chap. 4.

[15] M. A. Anisimov, *Critical Phenomena in Liquids and Liquid Crystals* (Gordon and Breach Science Publishers, Philadelphia, 1991).

[16] H. J. Coles, Mol. Cryst. Liq. Cryst. **49**, 67 (1978).

[17] P. P. Karat and N. V. Madhusundana, Mol. Cryst. Liq. Cryst. **40**, 239 (1977).

[18] P. E. Cladis and M. Kleman, J. Phys. (Paris) **33**, 591 (1972); R. B. Meyer, Philos. Mag. **27**, 405 (1973).

[19] G. P. Crawford, R. Ondris-Crawford, S. Zumer, and J. W. Doane, Phys. Rev. Lett. **70**, 1838 (1993).

[20] Although C_P is measured experimentally, for liquid crystals, there is a negligible difference with respect to the theoretically predicted C_V, see Ref. [21].

[21] G. S. Iannacchione, Ph.D. thesis, Kent State University, 1993.

[22] J. Thoen, in *Phase Transitions in Liquid Crystals*, edited by S. Martellucci and A. N. Chester (Plenum, New York, 1992), Chap. 10.